JOURNAL OF AIRCRAFT
Vol. 43, No. 4, July–August 2006

Tip Vortex Control via an Active Trailing-Edge Tab

A. Panagakos* and T. Lee†
McGill University, Montreal, Quebec H3A 2K6, Canada

The effect of a movable trailing-edge tab on a tip vortex generated by an oscillating NACA 0015 wing was investigated at $Re = 1.86 \times 10^5$ by using a miniature triple hot-wire probe. Both upward and downward tab deflections, actuated with different start times and durations, were tested. The downward tab motion was most effective in displacing the vortex position. The earlier the actuation the larger the displacement. The upward tab motions were, however, found to be more effective in diffusing the tip vortex and rendered a significantly reduced peak tangential velocity and core circulation, compared to an uncontrolled baseline wing. The earlier and longer the upward tab actuations the lower the vortex core strength and peak tangential velocity. The vortex core radius was rather insensitive to the tab motion. The upward tab deflection, however, produced less induced drag compared to a downward deflection.

Nomenclature

b	=	(semi-)wing span
C_{Di}	=	induced drag coefficient, $=D_i/\frac{1}{2}\rho u_\infty^2 S$
C_l	=	section lift coefficient
c	=	airfoil chord
D_i	=	lift-induced drag
d_{miss}	=	miss distance
f_o	=	oscillation frequency
L	=	lift
l	=	span over which two-dimensional blade-vortex interaction occurs
Re	=	Reynolds number, $=u_\infty c/\nu$
r_c	=	vortex core radius
t	=	time
t_d	=	flap actuation duration
t_e	=	end of flap actuation
t_s	=	flap actuation start time
t_{ss}	=	steady-state time period
u	=	mean wake velocity
u_∞	=	freestream velocity
v	=	transverse mean velocity
v_θ	=	tangential velocity
w	=	spanwise mean velocity
x	=	streamwise distance
y	=	normal distance
α	=	angle of attack
α_m	=	mean angle of attack
$\alpha_{\max}$	=	maximum angle of attack
$\alpha_{\min}$	=	minimum angle of attack
α_{ss}	=	static-stall angle
Γ	=	circulation or vortex strength
Γ_c	=	core circulation
Γ_0	=	total circulation
Δ	=	$\Gamma_c c/(y_c+c)^2 u_\infty\vert_{\mathrm{controlled}} - \Gamma_c c/(y_c+c)^2 u_\infty\vert_{\mathrm{uncontrolled}}$
$\Delta\alpha$	=	oscillation amplitude
δ	=	flap deflection
ζ	=	streamwise vorticity
κ	=	reduced frequency, $=\pi f_o c/u_\infty$
ν	=	kinematic viscosity
ρ	=	fluid density
τ	=	phase angle, $=\omega t$

Subscripts

c	=	vortex core
d	=	pitch down
u	=	pitch up
∞	=	freestream

Introduction

WING-TIP vortices are caused by a pressure difference between the high-pressure region below the wing and the low-pressure region above the wing, which induces a circulatory motion over the wing-tip and results in an adverse influence on the wing aerodynamics. For rotorcraft, when these shed concentrated vortices interact with the trailing rotor blades, the unsteady pressure fluctuations induced on the blade surfaces generally lead to severe dynamic structural loading and impulsive blade-vortex-interaction (BVI) noise generation. The BVI noise is particularly evident and generally dominant during low-speed descent flight, as in landing approach and during maneuvers.

The rotorcraft BVI noise is a highly complex, three-dimensional, time-dependent phenomenon. In low-speed descent there can be multiple BVI events occurring on both the advancing and retreating sides of the rotor disk. Two important blade-vortex interaction extremes occur when the vortex is either normal, which affects a small spanwise portion of the airfoil, or parallel, which affects most of the airfoil and generates the greatest effect on BVI noise generation to the airfoil. Past experimental and computational results[1–7] had indicated that the more nearly parallel the tip vortex is to the blade at the time of interaction, the more intense the noise. Also, the blade-vortex interactions are highly dependent on the rotor's wake structure and trajectory.

Hardin and Lamkin[1] have showed theoretically that the severity of the acoustic pressure time history $p(x, t)$ produced by the BVI phenomenon can be expressed as

$$p(x, t) \approx \frac{\Gamma L l}{\rho_\infty d_{\mathrm{miss}}^2} \tag{1}$$

where x is the observer position in the airfoil fixed coordinate, Γ is the intensity of the incoming vortex, L is the lift of the blade (per unit length) at the time of interaction, d_{miss} is the miss distance of vortex and the interaction blade (which is controlled by the vortex trajectory), and ρ_∞ is the freestream density. Equation (1) clearly suggests that the miss distance appears to be the most influential BVI control parameter. However, even though the change in d_{miss}

Received 14 June 2005; revision received 29 September 2005; accepted for publication 30 September 2005.

*Graduate Research Assistant, Department of Mechanical Engineering.
†Associate Professor, Department of Mechanical Engineering. Member AIAA.

is believed to be the major factor in reducing the BVI noise, it is generally very difficult to control.

Various passive control devices[8–11] have been attempted to modify the shed vortex structure by changing the blade tip shape (e.g., Ogee tips), adding other aerodynamic surfaces mounted at the rotor tip (such as winglets, spoiler, stub/subwing, etc.), or blowing air along the vortex axis. These concepts are to spread out and diffuse the vortex so that the BVI is weakened to radiate less noise. On the other hand, active means such as higher harmonic control,[12] individual blade control, and trailing-edge tabs[13] have also been considered to reduce the blade-vortex interactions and the noise generation. Enenkl et al.[13] suggested that the way an active trailing-edge tab reduces noise and vibration can vary, depending mainly on flap chord, control frequency, and the blade's torsional stiffness. The details of the vortex flow characteristics, however, were not reported.

In addition, in forward flight the large increases in the helicopter rotor-blade torsional and control loads encountered during retreating blade continue to make dynamic stall and its control an important topic in rotorcraft engineering. The predominant feature of dynamic stall is the formation, convection, and shedding over the upper surface of the airfoil of an energetic leading-edge vortex (LEV), which induces a nonlinearly fluctuating pressure field and produces large transient variations in forces and moments that can be many times larger than their static counterparts. The rapid downstream convection of the LEV also produces a rapid aft movement of the center of pressure, which results in large nose-down pitching moments on the airfoil. This is the main adverse characteristic of dynamic stall that concerns the helicopter dynamicists. Once the LEV passes the airfoil trailing edge, the flow progresses to a state of poststall full separation over the upper surface, and an abrupt loss of lift is incurred. An excellent review on unsteady airfoils is given by McCroskey.[14] It is therefore believed that the transient LEV phenomenon will also impose a considerable influence on the behavior of the tip vortex. However, unlike the considerable experimental and numerical efforts made toward the understanding and control of the tip vortex generated by a fixed-wing tip, only limited results have been reported, to the authors' knowledge, on the tip vortex generated behind an oscillating wing.[15–17]

Ramaprian and Zheng[16] studied the near field of the tip vortex behind a square tipped oscillating NACA 0015 rectangular wing by using a three-component laser Doppler anemometer at $Re = 1.8 \times 10^5$ with $\alpha(t) = 10\,\text{deg} + 5\,\text{deg}\sin\omega t$ (i.e., the light-stall oscillation case[14,18]) and a reduced frequency κ of 0.1 for $0.16 < x/c < 2.66$. They reported that in the near field the average trajectory of the oscillating tip vortex was very nearly the same as for a static wing at the mean incidence, and that for $x/c > 0.7$ the normalized circulation distribution across most of the inner region of the vortex exhibited the same universal behavior as the vortex behind a static wing. Chang and Park[17] examined the hysteretic behavior of the wake behind a NACA 0012 airfoil oscillated with $\alpha(t) = 15\,\text{deg} + 15\,\text{deg}\sin\omega t$ (i.e., the deep-stall oscillation case[14,18]) at $\kappa = 0.09$ for $Re = 3.4 \times 10^4$ by using a triple hot-film probe at $x/c = 0.5$ and 1.5. They found that the size of the vortex core was larger, and that the peak tangential velocity and vortex strength were smaller during pitch down than during pitch up. The details of the vortex flow quantities, however, were not reported in their Note.

The objective of this study was to use a trailing-edge-tab (TET) flow-control actuator to control the strength, size, and trajectory of a tip vortex in the near field behind an oscillating NACA 0015 airfoil at $Re = 1.86 \times 10^5$. Four prescheduled TET motions were tested. The scheduled controls were superimposed on the sinusoidally oscillated airfoil. Both upward and downward tab deflections were tested. Special emphasis was placed on the characterization of the effects of TET actuation start time and duration and deflection amplitude on the strength, size, shape, and trajectory of the tip vortex. Phase-locked ensemble-averaged crossflow and axial-velocity fields, the vorticity distribution, and the turbulence structure of the vortex over one cycle of oscillation were also obtained using a miniature triple hot-wire probe. These measurements on the potential mitigation of the severity of the blade-vortex interactions were also discussed.

Experimental Methods

The experiment was conducted in the 0.9 m × 1.2 m × 2.7 m low-speed, suction-type wind tunnel at McGill University with a freestream turbulence intensity of 0.03% at $u_\infty = 14.2$ m/s. A square-tipped, rectangular, untwisted NACA 0015 airfoil, fabricated from solid aluminum, with a chord length c of 20.3 cm and a span b of 49.5 cm, was used as the test model. The wing model was mounted horizontally at the center of the wind-tunnel test section. A 40-cm-diam aluminum endplate with sharp leading edges was fixed to an end support located 20 cm from the sidewall of the test section. The gap between the wing and the endplate was kept at less than 1 mm to minimize the leakage flow through the gap. The origin of the coordinate was located at the trailing edge of the airfoil with x, y, and z in the streamwise, normal, and spanwise directions, respectively. The two-dimensional uniformity of the flow distribution over the airfoil model was checked by traversing a 5-μm normal hot-wire probe located at 30%c downstream from the leading edge of the airfoil and $y = 5$ mm above the airfoil. The nonuniformity was found to be ±3% of the freestream value. The freestream velocity u_∞ was fixed at 14.4 m/s, which rendered a chord Reynolds number of 1.86×10^5.

A specially designed four-bar linkage and flywheel oscillation mechanism, capable of oscillating the airfoil sinusoidally at various amplitudes and frequencies, mounted on the external of the wind tunnel was used in the present experiment (Fig. 1a). The oscillating airfoil was chosen so as to simulate the quasi-periodic first harmonic angle-of-attack variations that are found on helicopter rotor during low-speed forward flight. The mean angle of attack α_m was varied by changing the relative angle between the rotating shaft and the rocker-shaft connector. The oscillation amplitude $\Delta\alpha$ was varied by attaching the coupler at specific radial locations on the flywheel. The flywheel was attached directly to an Exlar model DXM340C servomotor driven by an Emerson model FX3161 PCM1 programmable motion controller. The oscillation frequency f_o was monitored in real time using a HP model 3581A spectral analyzer and was measured to an accuracy of ±0.02 Hz. The four-bar mechanism provided an output which was sinusoidal to within 2%. The airfoil pitch axis was located at the quarter-chord location. The instantaneous α of the airfoil and the phase reference signal $\tau = \omega t$ were recorded from both the servomotor feedback resolver and a potentiometer mounted on the servomotor shaft. For the TET control experiment, the airfoil was oscillated through the static-stall angle α_{ss} with $\alpha(t) = 14\,\text{deg} + 8\,\text{deg}\sin\omega t$ and $\kappa = 0.09$. Note that when the phase angle was within the range $-0.5\pi \le \tau \le 0.5\pi$, the airfoil was described to be in pitch up; when $0.5\pi \le \tau \le 1.5\pi$, the airfoil was said to be in pitch down. Also, in the following discussion, the suffix u is used to indicate pitch up when α is increasing, and d is used to indicate pitch down when α is decreasing.

The wing was equipped with a TET flow control system. A 25% trailing-edge tab, with a width of 13% span, of a simple-hinged type was activated and deactivated independently by a Futaba model S-3003 servomotor, located at the wing root, driven by a custom-built controller (Fig. 1a). The TET was actuated in response to the wing phase signal. The tab was located at the trailing edge, centered at 93.5% span position. The TET actuation employed a brief pulse and could be actuated at any desired time and instantaneous angle of attack. The pulse signal was represented by a constant ramp-up motion, remained steady briefly, and was followed by a constant ramp-down motion (Fig. 1b). The time required to deflect the tab was approximately $8\% f_o^{-1}$ (i.e., 8% of the time required for the wing to undergo one full cycle of oscillation) and varied between cycles by less than $0.5\% f_o^{-1}$. The TET actuation duration t_d, amplitude $\delta_{\max}$, and the start time t_s were tested independently to quantify their effects on the tip vortex flow structure. Both upward and downward tab deflections with $\delta_{\max} = \pm 5.3$ deg were tested. The magnitude of $\delta_{\max}$ was limited by the actuation frequency required by the oscillation frequency f_o of the main wing, as well as by the present TET actuation mechanism. Two different $t_s = -0.5\pi$ and 0.167π radians with $t_d = 35\%$ and $50\% f_o^{-1}$, corresponding to tab actuations initiated at $\alpha_u = \alpha_{\min} = 6$ deg and $\alpha_u = 15$ deg, and ended at $\alpha_u = \alpha_{\max} = 22$ deg and $\alpha_d = 15$ deg, respectively, were considered.

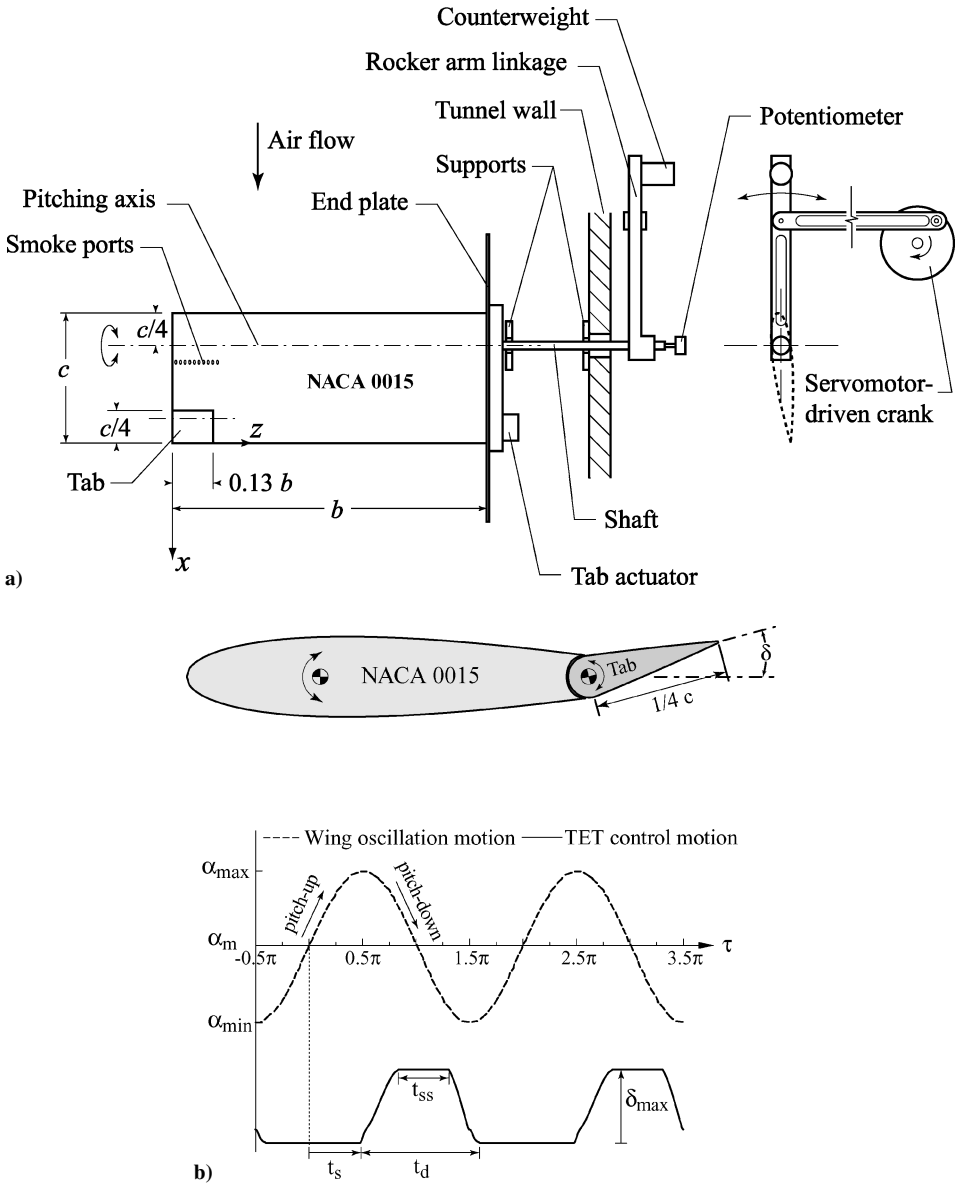

Fig. 1 Wing oscillation and TET control system: a) schematics of wing model and experimental setup and b) definition of flap actuation start time t_s, duration t_d, and amplitude $\delta_{\max}$.

Table 1 Values of TET motion profile

Case	$\delta_{\max}$, deg	t_s	t_s	$t_d(f_o^{-1})$, %[a]	t_{ss}/t_d[a,b]	t_e[c]	t_e[c]
1	+5.3	0.167π	15_u deg[d]	35	0.15	0.867π	15_d deg
2	−5.3	0.167π	15_u deg	35	0.15	0.867π	15_d deg
3	+5.3	-0.5π	6_u deg	50	0.41	0.50π	22_u deg
4	−5.3	-0.5π	6_u deg	50	0.41	0.50π	22_u deg

[a] $t_d = 50\%$ denotes 50% of the oscillation period.
[b] t_{ss} = steady-state time period.
[c] t_e denotes the end of the flap actuation duration.
[d] 15_u deg denotes $\alpha = 15$ deg during pitch up.

The start time $t_s = 0.167\pi$, corresponding to a flap actuation initiated at $\alpha_u = 15\,\text{deg} > \alpha_{ss} = 14.5$ deg, was chosen to allow the actuation of the tab at around the onset of flow reversal during the pitch-up motion, while the $t_s = -0.5\pi$ case corresponded to a TET actuated at the beginning of the pitch-up motion. Details of the parameters describing the flap actuation profile in various units are given in Table 1.

The instantaneous velocities were subsequently ensemble averaged over 40–80 oscillating cycles to obtain phased-locked averages of the flow properties at various phase positions during the cycle. A miniature triple hot-wire probe (Auspex Model AVEP-3-102 with a measurement volume of 0.5 mm^3) was used to measure the mean and fluctuating velocity components. The triple hot-wire probe were calibrated in situ, following the calibration procedures described by Chow et al.,[19] before the installation of the model. The hot-wire signals were sampled at 500 Hz and were recorded on a PC through a 16-bit A/D converter board. Probe traversing was achieved through a custom-built computer-controlled traversing system. The three-dimensional velocities downstream of the trailing edge of the wing were measured in planes perpendicular to the freestream velocity at $x/c = 2.0$. Data planes taken in the near field of the wing models had 56×56 measuring grid points with an increment of $\Delta y = \Delta z = 3.2$ mm. The maximum experimental uncertainties in the results reported have been estimated as follows[20]: mean velocity 3.5%, vorticity component 8%, vortex radius 4%, and velocity fluctuation 3%.

Results and Discussion

As discussed in the first section, past investigations have shown that the change in the miss distance between the oncoming vortex and the interaction blade seems to be the major factor in reducing the blade-vortex interactions and BVI noise. Also, it is less detrimental if the tip vortex can be somehow altered so that its strength is reduced or its core size substantially increased. The effect of TET motion on

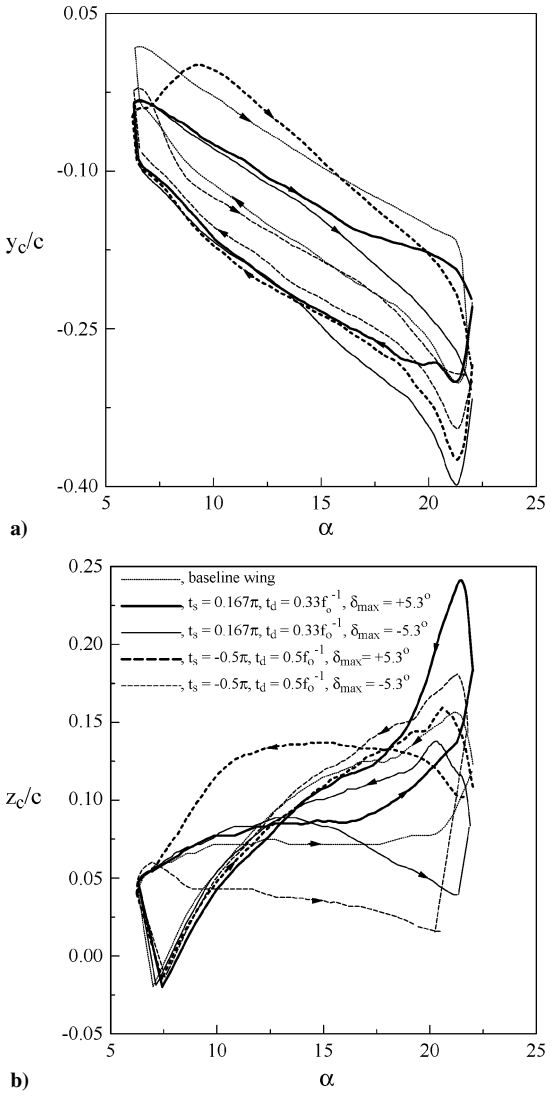

Fig. 2 Dynamic loops of vortex center position.

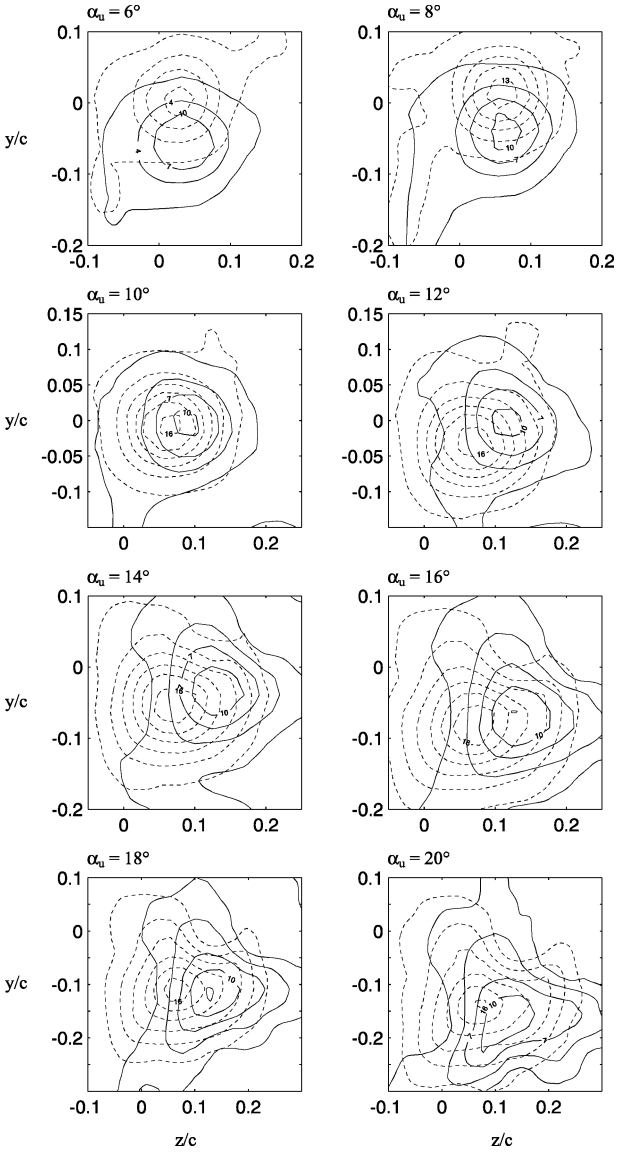

Fig. 3 Isocontour of normalized vorticity: ——, TET control with $t_s = -0.5\pi$; $t_d = 0.5f_o^{-1}$, and $\delta_{max} = +5.3$ deg; . . . . , baseline wing. Constant $\zeta c/u_\infty$ increment of 3.

the phase-resolved tip vortex position was therefore examined first and is presented in Fig. 2. Also shown in Fig. 2 is the uncontrolled, or baseline, wing data.

It is evident that both upward and downward TET motions always favorably influenced the d_{miss} to various levels, depending on the magnitudes of t_s and t_d. The vertical position y_c of the vortex center was significantly shifted further vertically downward below the wing as α was increased (Fig. 2a), except for case 3 for $\alpha_u = 10$ to 15 deg, compared to a baseline wing, which translates, equivalently, into a reduced blade-vortex interaction with lessened unsteady blade pressure fluctuations and, subsequently, a lowered noise emission [as indicated by Eq. (1)]. An opposite movement of the vortex center was observed as α was decreased. The vortex center was taken as the location of maximum local vorticity. The vertical displacement of the vortex center during pitch down, especially in the vicinity of $\alpha_{\max}$, was particularly pronounced. The downward tab deflection was more effective in displacing the vortex vertically, compared to the upward deflection. The earlier the TET actuation the larger the vortex displacement. The downward TET motion with $t_s = -0.5\pi$ and $t_d = 0.5\,f_o^{-1}$, representing a tab deflection covering the entire upstroke motion, produced a maximum displacement of the vortex position, as well as a narrowest hysteresis (well below that of a baseline wing) in y_c between pitch up and pitch down. Figure 2b shows that for upward TET deflection the vortex was generally shifted further inboard with increasing t_d and an earlier TET initiation. For downward deflection, the spanwise position of the vortex center z_c was, however, observed to be shifted further outboard, especially during the pitch-up motion of the wing. The larger the downward deflection the more significant the outboard shifting of the vortex center. The TET motion was more effective in displacing the vortex in the vertical direction than in the horizontal direction.

The TET motion on the changes in the tip vortex structure, in addition to the vortex position, can be best reflected from the variation of the isovorticity contours (Fig. 3) and the strength of the vortex (Fig. 4). Figure 3 shows the typical composite plots of the nondimensional vorticity contour for an upward TET actuated at $t_s = -0.5\pi$ (or at $\alpha_u = 6$ deg) and $t_d = 0.5\,f_o^{-1}$ (i.e., the tab actuation ended at $\alpha_u = 22$ deg), overlapped with those of a baseline wing, at selected α. For a baseline wing, the vortex at the oscillating wing tip appeared to be more tightly wound and had higher contour levels than the upward TET control case. As expected, an upward deflected tab led to a substantial reduction in the vorticity contour levels and vortex strength (Fig. 4) because much of the lift generated in the tip region was destroyed compared to a baseline wing. The upward tab motion also led to a reduced local angle of attack, or equivalently the tip pitch angle, through the TET-induced negative camber effects, especially in the trailing-edge region. The circulation, or vortex strength, was calculated by the area integral over vorticity. The area integral was evaluated by summing the vorticity multiplied with the incremental area of the measuring grid.

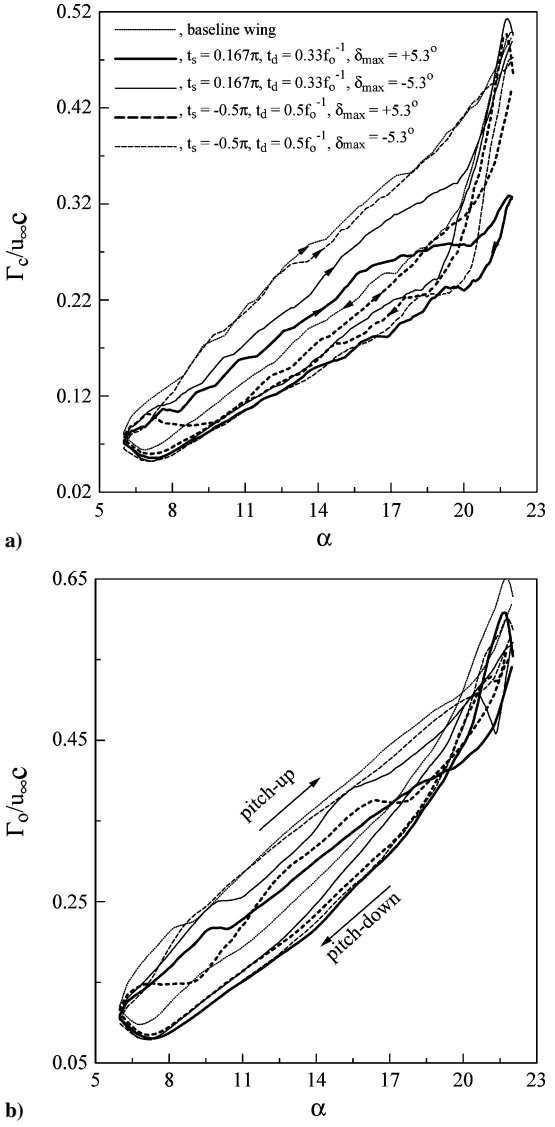

Fig. 4 Dynamic loops of total and core circulation.

Also, note that because of the convection time required for a tip-vortex flow structure to propagate from the wing to the downstream location of the sensor, there is a phase lag between any instantaneous sensor reading and the position of the wing at that instant. By assuming that within the streamwise length scale considered any streamwise distortion of the flow structure that occurs is negligible and that the convection speed u_{conv} is constant, the angle of attack through which the wing has swept during the convection time can be directly calculated. In the present experiment, u_{conv} was approximated as the upper-bound freestream speed because it resulted in the smallest phase lag correction; a phase lag compensation scheme suggested by Chang and Park.[17] Compensated and uncompensated angles of attack in degrees are summarized in Table 2. The measurements reported in this study were phase lag compensated by letting $u_{\text{conv}} = u_\infty$.

Figure 4 also clearly demonstrates the hysteretic property existing in the dynamic Γ_c (core circulation) and Γ_0 (total circulation) loops between pitch up and pitch down. For an oscillating wing with and without TET control, the values of Γ_c and Γ_0 always increased with increasing α and had higher circulation at a given α during pitch up than during pitch down. The increase-decrease trend observed in Γ during pitch up and pitch down was found to be similar to the behavior of the dynamic-C_l loop.[18] The vortex strength was reduced to a much lesser extent during pitch down, compared to during pitch up, because during pitch down the TET was completely embedded in a largely separated flow of weaker activity. The earlier and longer upward tab actuations are, the lower the vortex core circulation. The

Table 2 Compensated and uncompensated angles of attack in degrees

Pitch up		Pitch down	
Uncompensated	Compensated	Uncompensated	Compensated
6	6	22	21.79
7	6.59	21	21.62
8	7.19	20	21.00
9	7.82	19	20.35
10	8.49	18	19.65
11	9.22	17	18.89
12	10.01	16	18.07
13	10.87	15	17.17
14	11.81	14	16.19
15	12.83	13	15.13
16	13.93	12	13.99
17	15.10	11	12.78
18	16.35	10	11.51
19	17.65	9	10.18
20	18.99	8	8.81
21	20.38	7	7.41
22	21.79	6	6

degree, or level, of the hysteresis loop of Γ_c was also found to be greatly reduced with longer t_d and earlier t_s. The observed substantial reduction in Γ_c, especially during pitch up, also suggests that the upward TET deflections were very effective in alleviating the strength of a tip vortex, or equivalently blade-vortex interactions, by virtue of the increased core radius and/or the degree of spread of the vorticity. The reduction of the total circulation for an oscillating wing with TET control was, however, found to be of a much lesser extent compared to the significant reduction observed in the core circulation.

Figures 5a and 6a further indicate that the most noticeable quality, in addition to the reduction in the core vortex strength, was the lack of high rotational/tangential velocities and vorticity in the center region of the tip vortex as a result of the unloading of the tip region by an upward TET motion. The substantial reduction in the peak tangential velocity $v_{\theta\text{peak}}$ (Fig. 5a) and maximum vorticity ζ_{peak} (Fig. 6a), especially during pitch up, was accompanied by an increased core radius r_c (Fig. 5d) for $t_s = -0.5\pi$ and $t_d = 0.5f_o^{-1}$ with $\delta_{\max} = +5.3$ deg. Both upward and downward tab deflection led to a substantial reduction in $v_{\theta\text{peak}}$ and ζ_{peak} during pitch up and, to a much lesser extent, during pitch down. Similar to a baseline oscillating wing, the peak tangential velocity and core vorticity and radius had larger values during pitch up than during pitch down. It appears that the earlier and longer the TET actuation the larger the reduction in $v_{\theta\text{peak}}$ and ζ_{peak} was observed based on the data acquired. The effect of the TET motion on the core radius was generally found to be less noticeable, within measurement error, except in the vicinity of $\alpha_{\max}$ (Figs. 5b, 5c and 5e). The observed increase in r_c in the high-α range (Figs. 5c and 5e) suggests that the effect of a downward TET motion was most pronounced during the transient LEV and the poststall flow processes. Note that for cases (i.e., in the vicinity of $\alpha_{\max}$) when the vortex was irregularly shaped, the core radius r_c was calculated as the average distance between the vortex center and the location of $v_{\theta\text{peak}}$ along a line radiating from the vortex center.

Figure 6b shows that for an oscillating wing with TET control the axial core velocity u_c was always wake like (of lower value than a baseline wing) during pitch down and was smaller at a given α during pitch up than during pitch down, similar to a baseline wing. The downward TET deflection, however, had larger axial-velocity deficits compared to an upward-deflected TET. During pitch up, the variation of u_c, however, was characterized by a sharp rise and drop (well above and below the freestream value, respectively) during the upstream movement of the flow reversal and the subsequent formation and convection of a LEV. The local maximum values of the jet-like core axial velocity (occurred at around the dynamic-stall angle) were found to be decreased for an oscillating wing with TET control, compared to a baseline wing. For TET-controlled cases, the later the TET actuation the lower maximum u_c. The variation in the core flow characteristics, in particular the

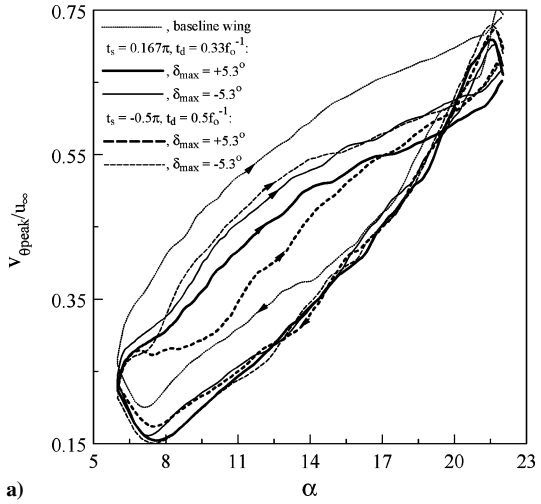

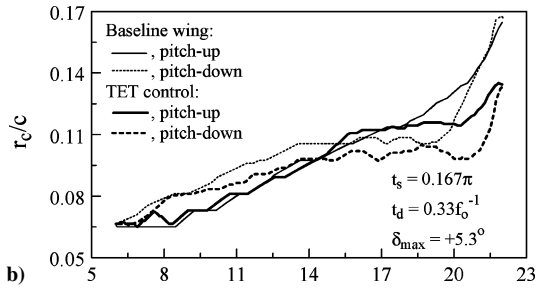

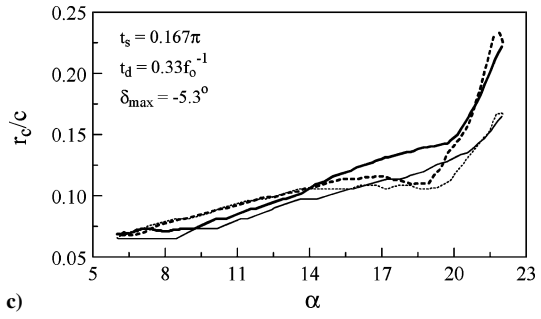

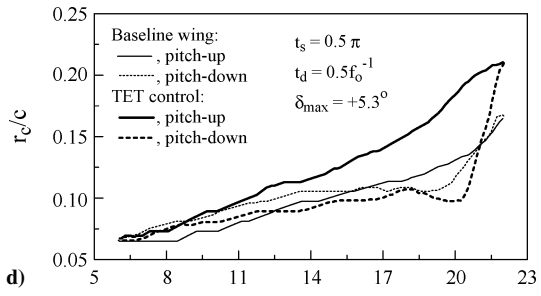

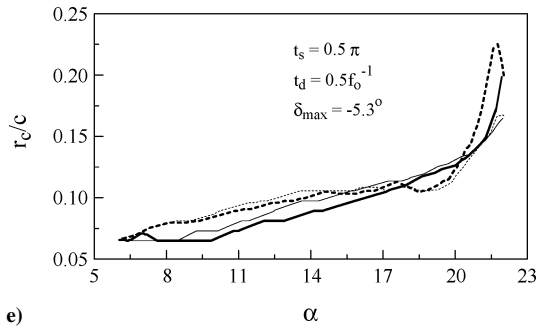

Fig. 5 Dynamic loops of peak tangential velocity and vorticity.

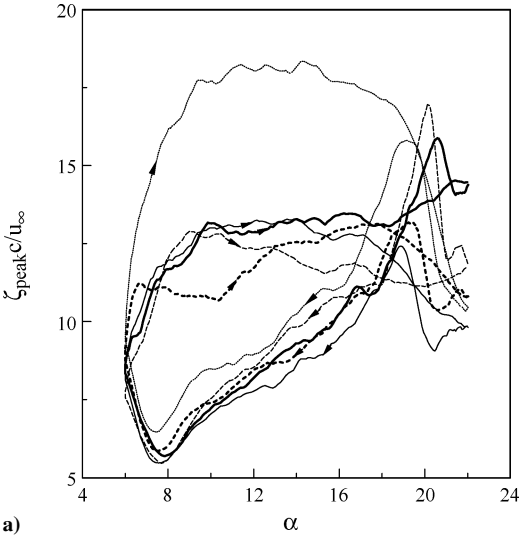

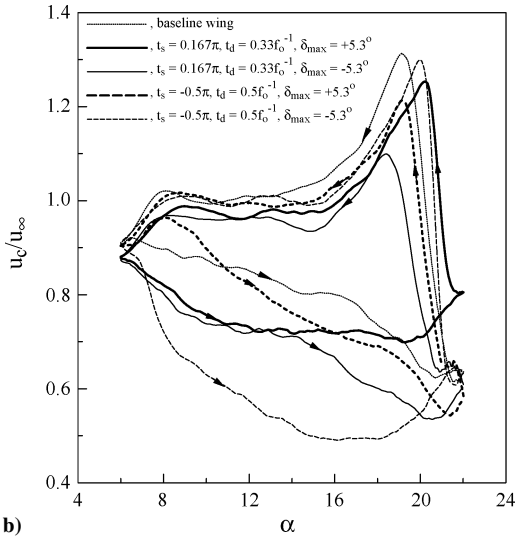

Fig. 6 Variation of core radius and axial velocity over one oscillation cycle.

values of Γ_c and y_c, with TET control also provides a comparative assessment of the potential for BVI noise reduction utilizing Eq. (1) (Fig. 7). Figure 7 shows that for the four typical TET control cases tested, an upward-deflected TET initiated at $t_s = 0.167\pi$ with $t_d = 0.33\,f_o^{-1}$ provided a persistent reduction in BVI noise generation (i.e., $\Delta < 0$ based on the measured Γ_c and y_c) throughout the entire oscillation cycle in comparison to a generally positive Δ for a downward TET at the same t_s and t_d. The values of Δ were defined as $\Delta = \Gamma_c c/(y_c + c)^2 u_\infty|_{\text{controlled}} - \Gamma_c c/(y_c + c)^2 u_\infty|_{\text{uncontrolled}}$. Note the considerable increase and decrease in Δ presented for $\alpha_u = 18$ deg to $\alpha_d = 18$ deg, which corresponded to the onset of the flow reversal and the end of the stall flow processes, respectively. Figure 7 also shows that for an upward TET actuated at $t_s = -0.5\pi$ with $t_d = 0.5\,f_o^{-1}$ a large improvement in Δ, except in the vicinity of $\alpha_{\max}$, during pitch up, while an improved Δ was observed during pitch down for a downward TET at the same t_s and t_d.

Finally, the lift-induced drag coefficient C_{Di} was also computed, based on the vorticity inferred from the measured velocity field, by using the Maskell induced drag during one oscillation cycle. The vw-crossflow velocity vectors within the measurement plane were decomposed into a stream function $\psi(y, z)$ and a velocity potential $\phi(y, z)$ with the imposed boundary conditions requiring both ψ and ϕ to be zero on the edges of the measurement plane. The lift-induced drag was then obtained by

$$D_i = \frac{1}{2}\rho_\infty \iint_{S_\zeta} \psi\zeta \,\mathrm{d}y\,\mathrm{d}z - \frac{1}{2}\rho_\infty \iint_{Sl} \phi\sigma \,\mathrm{d}y\,\mathrm{d}z \qquad (2)$$

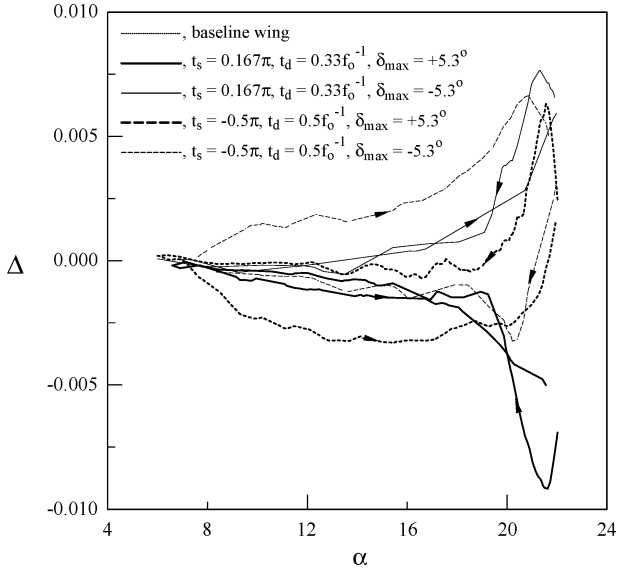

Fig. 7 Comparative assessment of the potential of BVI noise reduction utilizing Eq. (1). $\Delta = \Gamma_c c/(y_c + c)^2 u_\infty|_{\text{controlled}} - \Gamma_c c/(y_c + c)^2 u_\infty|_{\text{uncontrolled}}$.

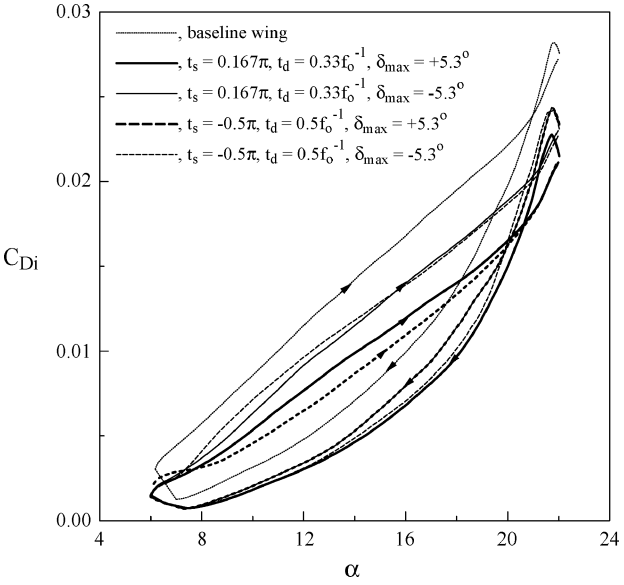

Fig. 8 Lift-induced drag coefficient.

where ζ is the vorticity, the surface S_ζ is the region within $S1$ where the vorticity is nonzero, $\sigma\,(=\partial v/\partial y + \partial w/\partial z)$ is a source term, and the flow is incompressible. Figure 8 shows that similar to the observed variation in $v_{\theta\text{peak}}$ and ζ_{peak} with α (Figs. 5a and 6a) the lift-induced drag coefficient was higher during pitch up than during pitch down and had values lower than a baseline wing. The upward-deflected TET produced less C_{Di} compared to a downward TET motion. The earlier the TET actuation is the lower the lift-induced drag. In other words, the downward TET deflection delayed the trailing-edge flow separation and the dynamic lift stalling and thus rendered an increase in the lift force, compared to a baseline wing, but at the price of an increased C_{Di}.

Conclusions

The scheduled TET controls, superimposed on a sinusoidally oscillating NACA 0015 airfoil, on the near-field tip vortex flow structure were investigated at $Re = 1.86 \times 10^5$. The downward TET deflection was found to be most effective in displacing the vortex position. The earlier the actuation was, the larger the displacement. The upward TET motions, however, were found to be more effective in diffusing the tip vortex and significantly reduced its peak tangential velocity and core circulation, compared to an uncontrolled baseline wing. The earlier and longer the upward TET actuations were, the lower the vortex core strength $v_{\theta\text{peak}}$ and ζ_{peak}. The effect of TET motion on the vortex core radius, however, was much less noticeable, compared to the significant changes observed in $v_{\theta\text{peak}}$, Γ_c, and the vortex trajectory. The lift-induced drag was always decreased compared to a baseline wing. The upward TET deflection, however, produced less C_{Di} compared to a downward TET deflection. The observed favorable changes in the core circulation, peak rotational velocity, and the displacement of the vortex position will certainly lead to a less detrimental blade-vortex interaction. Additional measurements are needed to reinforce the findings reported here. Implementation of a closed-loop control system with different TET control parameters is needed. In addition, both off- and on-surface flow measurements and visualizations are needed to better understand the phenomena reported here.

Acknowledgment

This work was supported by the Natural Science and Engineering Research Council of Canada. D. Birch is thanked for his help with the experiment.

References

[1]Hardin, J. C., and Lamkin, S. L., "Concepts for Reduction of Blade/Vortex Interaction Noise," *Journal of Aircraft*, Vol. 24, No. 2, 1987, pp. 120–125.

[2]Booth, E. R., "Experimental Observations of Two-Dimensional Blade-Vortex Interaction," *AIAA Journal*, Vol. 28, No. 8, 1990, pp. 1353–1359.

[3]Straus, J., Renzoni, P., and Mayle, R. E., "Airfoil Pressure Measurements During a Blade Vortex Interaction and a Comparison with Theory," *AIAA Journal*, Vol. 28, No. 2, 1990, pp. 222–228.

[4]Lee, S., and Bershader, D., "Head-on Parallel Blade-Vortex Interaction," *AIAA Journal*, Vol. 32, No. 1, 1994, pp. 16–22.

[5]Brooks, T. F., Booth, E. R., Boyd, D. D., Niesl, G. H., and Streby, O., "Analysis of a Higher Harmonic Control Test to Reduce Blade Vortex Interaction Noise," *Journal of Aircraft*, Vol. 31, No. 6, 1994, pp. 1341–1349.

[6]Tung, C., Kube, R., Brooks, T. F., and Rathier, G., "Prediction and Measurement of Blade-Vortex Interaction," *Journal of Aircraft*, Vol. 35, No. 2, 1998, pp. 260–266.

[7]Wilder, M. C., and Telionis, D. P., "Parallel Blade-Vortex Interaction," *Journal of Fluids and Structures*, Vol. 12, 1998, pp. 801–838.

[8]Tangler, J. L., "Experimental Investigation of the Subwing Tip and Its Vortex Structure," NASA CR-3058, 1978.

[9]Liu, Z., Russell, W., Sankar, L. N., and Hassan, A. A., "A Study of Rotor Tip Vortex Structure Alternation Techniques," *Journal of Aircraft*, Vol. 38, No. 3, 2001, pp. 473–477.

[10]Muller, R. H. G., "Winglets on Rotor Blades in Forward Flight—A Theoretical and Experimental Investigation," *Vertica*, Vol. 14, No. 1, 1990, pp. 31–46.

[11]Gerontakos, P., and Lee, T., "Effect of Winglet Dihedral on a Tip Vortex," *Journal of Aircraft*, Vol. 43, No. 1, 2006, pp. 125–131.

[12]Nguyen, K., "Active Control of Helicopter Blade Stall," *Journal of Aircraft*, Vol. 35, No. 1, 1998, pp. 91–98.

[13]Enenkl, B., Kloppel, V., Preibler, D., and Janker, P., "Full Scale Rotor with Piezoelectric Actuated Blade Flaps," *28th Europe Rotorcraft Forum*, Paper 89, Bristol, England, U.K., Sept. 2002.

[14]McCroskey, W. J., "Unsteady Airfoils," *Annual Review of Fluid Mechanics*, Vol. 14, 1982, pp. 285–311.

[15]Freymuth, P., Finaish, F., and Bank, W., "Visualization of Wing-Tip Vortices in Accelerating and Steady Flow," *Journal of Aircraft*, Vol. 23, No. 9, 1985, pp. 730–733.

[16]Ramaprian, B. R., and Zheng, Y., "Near Field of the Tip Vortex Behind an Oscillating Rectangular Wing," *AIAA Journal*, Vol. 36, No. 7, 1998, pp. 1263–1269.

[17]Chang, J. W., and Park, S. O., "Measurement in the Tip Vortex Roll-up Region of an Oscillating Wing," *AIAA Journal*, Vol. 38, No. 6, 2000, pp. 1092–1095.

[18]Lee, T., and Gerontakos, P., "Investigation of Flow Over an Oscillating Airfoil," *Journal of Fluid Mechanics*, Vol. 512, 2004, pp. 313–341.

[19]Chow, J. S., Zilliac, G. G., and Bradshaw, P., "Mean and Turbulence Measurements in the near Filed of a Wingtip Vortex," *AIAA Journal*, Vol. 35, No. 10, 1997, pp. 1561–1567.

[20]Birch, D., and Lee, T., "Structure and Induced Drag of a Tip Vortex," *Journal of Aircraft*, Vol. 41, No. 5, 2004, pp. 1138–1145.